IET Computer Vision

Review Article

IET Journals
The Institution of Engineering and Technology

Fusion of structural and textural features for melanoma recognition

ISSN 1751-9632
Received on 5th April 2017
Revised 22nd August 2017
Accepted on 4th October 2017
doi: 10.1049/iet-cvi.2017.0193
www.ietdl.org

Faouzi Adjed[1,2], Syed Jamal Safdar Gardezi[2], Fakhreddine Ababsa[1], Ibrahima Faye[2] ✉, Sarat Chandra Dass[2]

[1]*Laboratoire IBISC EA 4526, Université D'Evry Val d'Essonne, 91020 Evry, France*
[2]*Center for Intelligent Signals and Imaging Research, Department of Fundamental and Applied Sciences, University Tecknologi PETRONAS, Bandar Seri Iskandar 32610, Malaysia*
✉ *E-mail: ibrahima_faye@utp.edu.my*

Abstract: Melanoma is one the most increasing cancers since past decades. For accurate detection and classification, discriminative features are required to distinguish between benign and malignant cases. In this study, the authors introduce a fusion of structural and textural features from two descriptors. The structural features are extracted from wavelet and curvelet transforms, whereas the textural features are extracted from different variants of local binary pattern operator. The proposed method is implemented on 200 images from PH^2 dermoscopy database including 160 non-melanoma and 40 melanoma images, where a rigorous statistical analysis for the database is performed. Using support vector machine (SVM) classifier with random sampling cross-validation method between the three cases of skin lesions given in the database, the validated results showed a very encouraging performance with a sensitivity of 78.93%, a specificity of 93.25% and an accuracy of 86.07%. The proposed approach outperforms the existing methods on the PH^2 database.

1 Introduction

Melanoma is amongst one of the most dangerous cancers. An estimated 2–3 million people suffer from non-melanoma, and around 132,000 of melanoma cases are diagnosed globally every year [1–3]. Skin cancer represents ∼1.6% of the total number of cancer worldwide [3, 4]. Its treatment needs chemotherapy and radiotherapy such as other cancers types such as breast cancer, blood cancer, brain tumour or lung cancer when reached in metastasis state [3, 5]. To avoid these painful procedures, and for a successful treatment, early detection is one of the most reliable solutions.

Skin cancer detection has been an attractive topic to researchers since 1984 in computerised analysis of pigment skin lesions (PSLs). A survey by Korotkov and Garcia [6] summarise the issues in dermoscopic and clinical images of PSL. Their work provides good background information on the nature of skin lesions, imaging modalities and techniques, procedures for clinical diagnosis and automated melanoma diagnosis systems. Over the years, many researchers have proposed various methods/techniques in computer-aided diagnosis (CAD) systems to improve the performance metrics such as accuracy, sensitivity and specificity, area under curve and/or receiver operator curve (ROC) as explained and detailed by Celebi *et al.* [7]. Like all other CAD systems in medical image analysis, the skin images also undergo image acquisition, preprocessing, segmentation, feature extraction and finally, classification step.

In the current work, we explore a new approach for discrimination of melanoma lesions using multiresolution analysis such as wavelet and curvelet coefficients, combined with local binary pattern (LBP) operator applied on dermoscopic images. The developed approach uses the fusion of different features extracted from various operators. The structural features are obtained from multiresolution analyses (wavelet and curvelet coefficients) which are used to discriminate the structures as borders, dots and streaks. On the other side, the textural features computed by LBP operator are used to discriminate the local variation of colours, the pigment network etc. Later, these features are fused in multiple combinations to investigate the influence of each combination in the performance of melanoma detection.

In this paper, we also investigate a deep statistical representativeness and the inference representation of the database used, which is important for the confidence of the obtained results. We also applied Dullrazor [8] software as a preprocessing step to remove hairs.

The rest of this paper is organised as follows: Section 2 presents a brief literature review of the methods used in skin cancer recognition for each step of CAD system. Section 3 provides the mathematical background of wavelet and curvelet transforms, and the LBP operator. Section 4 presents the proposed method of feature extraction. The used database is presented and statistically analysed in Section 5. Section 6 presents the experimental works and the details of features used followed by the experimental results Section 7, where the results of each configuration are presented and the analysis of the results discussed. Finally, the conclusion is depicted in Section 8.

2 Literature review

In the literature, several researchers have focused on developing CAD systems for skin cancer detection. In hospitals, to detect the melanoma tissues, patients generally undergo a skin examination using the skin surface microscopy techniques commonly known as dermoscopy [9]. To measure the severity of skin deformation, physicians often use scoring methods such as the ABCD rule [10] or the 7-point checklist [11] for diagnosis and detection of melanoma. As Image processing techniques, the contributions of different papers in the literature are in image preprocessing, segmentation, feature extraction and/or classification.

For preprocessing of melanoma images, many methods proposed in the literature focused on hair removing and contrast enhancement. Once such methods, named Dullrazor, was introduced by Lee *et al.* [8] to remove hair and image artefacts. It is one of the most widely known software in dermoscopic images [6]. With a similar objective, Abbas *et al.* [12] proposed a matched filtering with first derivative-of-Gaussian method for hair detection. This method shows accurate results, but the multitude of parameters complicates its implementation. Applied on 100 dermoscopic images, the method shows a detection accuracy of 93.3%. Barata *et al.* [13] used a bank of directional filters and

Table 1 Summary of the characteristics of PH^2 database

Database characteristics		Common Nevus (80)	Atypical Nevus (80)	Melanoma (40)
asymmetry	fully symmetric	96.25% (77)	43.75% (35)	12.5% (5)
	symmetric in one axis	2.5% (2)	33.75% (27)	5% (2)
	fully asymmetric	1.25% (1)	22.5% (18)	82.5% (33)
pigment network	typical	100% (80)	3.75% (3)	2.5% (1)
	atypical	0% (0)	96.25% (77)	97.5% (39)
dots/globules	absent	36.25% (29)	50% (40)	45% (18)
	typical	57.5% (46)	10% (8)	0% (0)
	atypical	6.25% (5)	40% (32)	55% (22)
streaks	absent	98.75% (79)	80% (64)	67.5% (27)
	present	1.25% (1)	20% (16)	32.5% (13)
regression area	absent	100% (80)	95% (76)	47.5% (19)
	present	0% (0)	5% (4)	52.5% (21)
blue-whitish veil	absent	100% (80)	92.5% (74)	25% (10)
	present	0% (0)	7.5% (6)	75% (30)
colour	one colour	42.5% (34)	25% (20)	0% (0)
	two colours	53.75% (43)	63.75% (51)	32.5% (13)
	three colours	3.75% (3)	11.25% (9)	27.5% (11)
	four colours	0% (0)	0% (0)	32.5% (13)
	five colours	0% (0)	0% (0)	7.5% (3)

Partial Differential Equation (PDE)-based interpolation for hair detection and inpainting, respectively. Then, the authors applied a bank of directional filters and connected component analysis to detect the lines of pigment network. Recently, Koehoorn *et al.* [14] proposed a new approach based on thresholding set decomposition and morphological analysis using gap-detection by multi-scale skeletons. They applied their method on more than 300 skin images and compared visually their results to the literature. They also compared the execution time of these methods. Mirzaalian *et al.* [15] proposed an alternative approach to detect hair in dermoscopic images using the measurement of turbulence quaternion [16] and dual matched filters for hair detection and suppression. On a database of 40 dermoscopic images and 94 synthetic images, the results obtained are, for segmentation, 86 and 85% of accuracy for dermoscopic and synthetic images, respectively.

Once the preprocessing step is completed, the next challenging task is the segmentation of melanocytic lesions from the processed images. It refers to separate an image into disjoint homogeneous regions respecting some properties such as luminance, colour and texture. This procedure is detailed in Celebi *et al.* [17] and completed in [7], where the authors classified several methods of image segmentation explored in the literature into different categories such as histogram thresholding, clustering, edge based etc. They also compared the recent border detection methods (50 methods), and concluded that half (25/50) of them use smoothing filters, and those based on thresholding are inherently robust against noises. The authors noted that two methods, clustering (19/50) and thresholding (18/50), are the most popular segmentation methods. Previously, Celebi *et al.* [18] used the Otsu thresholding method for lesion localisation. In Capdehourat *et al.* [19], Colour-based Otsu method was also used, which is simpler and significantly faster for some cases. Safi *et al.* [20] used a total variation method developed by Li *et al.* [21], which is the generalisation of Chan and Vese model [22]. The main idea is to minimise the convex energy of the image. The results of these methods are very encouraging. In a similar kind of study, an extension of Chan and Vese model to differentiate the melanoma and non-melanoma cases in skin cancer images is explored and presented in [23].

The feature extraction step plays a crucial role in CAD systems, because the classification and diagnosis depends on the types of features extracted and their discriminating power. There are several feature extraction methods in skin cancer research as in [20], where the authors used the idea of the Asymmetry, Border, Color, Diameter, Evolving (ABCDE) rule for extracting the image's features from the regions of interest (ROIs). In this rule, A is asymmetry, B is border, C stands for colour, D is diameter and E is elevation or evolving (less used in clinical treatment). A set of features are extracted by Celebi *et al.* [18] from multiple operators describing the shape such as asymmetry and compactness of the lesions, and colour features computing several statistical measures over channels and colour spaces. They also used textural features, where grey-level co-occurrence was employed. Multi-scale roughness descriptors were used by Clawson *et al.* [24], Capdehourat *et al.* [19] and Arroyo and Zapirain [4], where the authors computed important statistical features as variance, Hessian matrix and entropy. In [4], they extracted Gaussian features using different values of σ and spectral texture features. To select the best features, a decision tree by means rule was implemented to obtain the 23 most significant features from a total of 80 extracted features. Similarly, Barata *et al.* [9] compared the global/local texture and colour features to classify skin lesion. For smart-phone-based real-time systems, Abuzaghleh *et al.* [25] proposed fast Fourier transform (FFT) mixed with discrete cosine transform (DCT) applied on colour and shape for feature extraction.

Classification is the last step in the typical work-flow for the computerised analysis PSL images. The classification performance is often measured in terms of accuracy, sensitivity and specificity. The computation of these metrics is mostly used to compare the results. The most used classification and often explored by radiologist on ABCD criteria is scoring system by thresholds [6, 19], where the score is computed following the value and the weight attributed to each feature (see Table 1). They also used a 7-point checklist, which is another scoring system. The scores were divided into two parts, i.e. major criteria (atypical pigment network, blue-whitish veil and atypical vascular pattern) and minor criteria (irregular streaks, irregular pigmentation, irregular dots/globules and regression structures). The major criteria received two points and those lying under minor criteria were awarded one point [6, 19]. The classification is also done by thresholding for 7-point checklist.

In the literature, Maglogiannis and Doukas [26] enumerate many classifiers explored in different classification methods used in dermoscopy such as Support Vector Machine (SVM), artificial neural network, K-nearest neighbours, discriminant analysis), decisions trees, *K*-means, Bayesian classifiers and regression analysis. Celebi *et al.* [18] used SVM classifier on a database of 564 images, with a proportion of 15.6% melanoma and 84.4% benign, an area under the ROC of 0.9662 is obtained as results. Capdehourat *et al.* [19] applied their approach on 655 images of melanocytic lesions: 544 benign lesion and 111 malignant melanoma. The result obtained is 89% of specificity and 95% of sensitivity using AdaBoost/C5.4 approach. They compared their

method with ABCD rule and 7-point checklist. The objective of Arroyo and Zapirain [4] is to detect typical and atypical networks, using high-level design which is composed of two main blocks, the machine learning process and the searching of pattern structures. They used C4.5 algorithm on 220 images (120 without reticular pattern and 100 with such structure), the sensitivity is 86% and the specificity is 81.67%.

Recently, Codella *et al.* [27] combine deep learning, sparse coding and SVM learning algorithms. On a database of 2624 skin images from International Skin Imaging Collaboration (ISIC) archive database, a two-fold cross-validation is applied for classification. The result obtained shows 93.1% of accuracy, 94.9% of sensitivity and 92.2% of specificity. One of the drawbacks of Codella *et al.* [27] study is that they chose a particular set of lesions for their approach which can be considered as statistically biased. Barata *et al.* [28] used four algorithms to extract colour constancy (Gray World, max-Red Green Blue (RGB) color model, Shady of Gray and General Gray World). SVM classifier with the χ^2 kernel is used for classification on two different databases, PH^2 and Interactive Atlas of Dermoscopy (Skin Database) (EDRA). The results obtained show the best performance on PH^2 database, with an accuracy of 84.3%, a sensitivity of 92.5% and a specificity of 76.3%. Abuzaghleh *et al.* [25] used colour and shape geometry features using FFT and DCT. SVM classifier is used on PH^2 database for 75% for training and 25% for test. The results showed an accuracy of 90.6%.

From the aforementioned methods, most of the developed methods consider only local or global features [4, 18, 24], and in other cases the authors used some special descriptors such as colour [28], pigment network and border irregularities [19]. In addition to that the majority of developed methods are based on ABCD rule or 7-point checklist methods, which are more visual scoring system than CAD system. For a fair comparison amongst the studies the database should be the same, which is not the case for many of these studies. Thus, from the literature, we suggest, three main items to aid the comparison of different proposed methods:

(i) The use of public databases, which could in addition to their private database.
(ii) The highlighting of all parameter details.
(iii) The results validation using statistical methods such as cross-validation.

Despite the several developed approaches, to our knowledge, there is no CAD system available for medical doctors that can perfectly discriminate melanoma. Thus, there is a need to explore new directions in skin cancer detection. In the current paper, we explore a set of features describing the local characteristics such as dots and network pigments, using LBP operator and global characteristics such as border irregularities and asymmetry, exploring multiresolution analysis using wavelet and curvelet transforms.

As evident from the literature, the detection of melanoma is a very challenging task in dermoscopic images. Thus, in the current paper, we present an approach to distinguish between the benign and malignant lesions. Multiresolution techniques, e.g. wavelet and curvelet provide shape representation of lesions by finding the borders and streaks in skin cancer image, while LBP operator is proposed to find all the local variations in colour and skin pigments. This paper presents an automatic set of features describing benign and malignant lesions. It aims at performing also between common, atypical and melanoma cases. The approach is performed and validated on a free public dataset of 200 dermoscopic images and all details are highlighted. Two comparisons are done, intermediary one which is performed between different combinations of textural and structural features, then, we compared the obtained results to the ones achieved in the literature using the same public database.

3 Mathematical tools

Sections 3.1–3.3 introduce the mathematical background of wavelet, curvelet transforms and LBP operator, respectively, which are implemented in the current study for the extraction of features.

3.1 Wavelet transform

Wavelet transform (WT) was introduced by Grossmann and Morlet [29] using translation and dilations on square integrable function $\psi \in L^2(\mathbb{R})$. The WT is defined by the following formula:

$$\psi_{a,\,b}(x) = \frac{1}{\sqrt{a}}\psi\left(\frac{t-b}{a}\right) \tag{1}$$

where $a > 0$ defines the scale and b the shift parameter.

A multiresolution approximation of $L^2(\mathbb{R})$ is a sequence $(V_j)_{j\in\mathbb{Z}}$ of closed subspaces of $L^2(\mathbb{R})$, such that: $\{0\} \subset \cdots \subset V_1 \subset V_0 \subset V_{-1} \subset \cdots \subset L^2(\mathbb{R})$ where $\{\phi_j\}$ is the orthonormal basis of V_j [30] with

$$\phi_{j,\,k}(x) = \sqrt{2^j}\phi(2^j x - k) \quad k \in \mathbb{Z} \tag{2}$$

The subspaces …, W_1, W_0, W_{-1}, … design the orthogonal complements of the subspaces …, V_1, V_0, V_{-1}, … defined above, such that: $V_m \oplus W_m = V_{m-1}$.

In multiresolution analysis, the subspaces V_j are generated by the function $(\phi_{j,\,k})_{k\in\mathbb{Z}}$ and W_j are generated by $(\psi_{j,\,k})_{k\in\mathbb{Z}}$. Then, the subspace V_j represents the large scale (approximations) and W_j represents the small scale (details).

Let $f(x)$ be a one-dimensional (1D) discrete function as sequence of numbers, the discrete WT (DWT) coefficients are defined as

$$W_\phi(j_0,\,k) = \frac{1}{\sqrt{M}}\sum_{x=0}^{M-1} f(x)\phi_{j_0,\,k}(x) \tag{3}$$

$$W_\psi(j,\,k) = \frac{1}{\sqrt{M}}\sum_{x=0}^{M-1} f(x)\psi_{j,\,k}(x) \tag{4}$$

where $j > j_0$, M is power of 2 which ranges from 2 to $j-1$ and $W_\phi(j_0,\,k)$, $W_\psi(j,\,k)$ are the approximation coefficient and details coefficients, respectively. Using these coefficients, the signal function $f(x)$ can be reconstructed as

$$\begin{aligned} f(x) = {} & \frac{1}{\sqrt{M}}\sum_k W_\phi(j_0,\,k)\phi_{j_0,\,k}(x) \\ & + \frac{1}{\sqrt{M}}\sum_{j=j_0}^{\infty}\sum_k W_\psi(j,\,k)\psi_{j,\,k}(x) \end{aligned} \tag{5}$$

The implementation of WT was presented by Mallat [30] introducing a set of filters $(h_l)_{l\in\mathbb{Z}}$ and $(g_l)_{l\in\mathbb{Z}}$ where

$$\phi_{j,\,k} = \sum_l h_l \phi_{j+1,\,2k+l} \tag{6}$$

$$\psi_{j,\,k} = \sum_l h_l \psi_{j+1,\,2k+l} \tag{7}$$

and

$$h_l = (-1)^n g_{1-l} \tag{8}$$

Therefore, the approximation and details coefficients are computed.

In a 2D case, we have a scaling function $\phi(x,\,y)$ and three directional wavelets defined below:

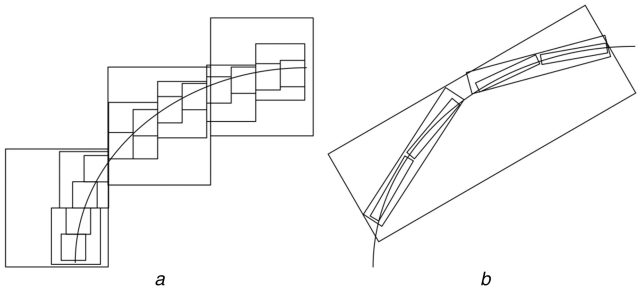

Fig. 1 *Comparison between*
(a) Wavelet and ***(b)*** Curvelet [35]

$$\begin{cases} \phi(x, y) = \phi(x)\phi(y) \\ \psi^{\mathrm{H}}(x, y) = \psi(x)\phi(y) \\ \psi^{\mathrm{V}}(x, y) = \phi(x)\psi(y) \\ \psi^{\mathrm{D}}(x, y) = \psi(x)\psi(y) \end{cases} \tag{9}$$

where ψ^{H}, ψ^{V} and ψ^{D} measure the horizontal, vertical and diagonal variation, respectively.

Finally, the wavelet coefficients of a given image I ($M \times N$) are computed using the following formulas:

$$W_{\phi}(j, k) = \frac{1}{\sqrt{MN}} \sum_{x=0}^{M-1} \sum_{y=0}^{N-1} I(x, y)\phi_{j,k}(x, y) \tag{10}$$

$$W_{\psi}^{\mathrm{H}}(j, k) = \frac{1}{\sqrt{MN}} \sum_{x=0}^{M-1} \sum_{y=0}^{N-1} I(x, y)\psi_{jk}^{\mathrm{H}}(x, y) \tag{11}$$

$$W_{\psi}^{\mathrm{V}}(j, k) = \frac{1}{\sqrt{MN}} \sum_{x=0}^{M-1} \sum_{y=0}^{N-1} I(x, y)\psi_{jk}^{\mathrm{V}}(x, y) \tag{12}$$

$$W_{\psi}^{\mathrm{D}}(j, k) = \frac{1}{\sqrt{MN}} \sum_{x=0}^{M-1} \sum_{y=0}^{N-1} I(x, y)\psi_{jk}^{\mathrm{D}}(x, y) \tag{13}$$

The potential of wavelet representation has had a wide impact in theory and in practise. It is used for non-linear approximation, compression and image denoising on different databases.

3.2 Curvelet transform

Curvelet transform is an extension of WT and it was introduced in 2000 by Candes and Donoho [31]. The same authors presented the second generation of curvelet [32], known as the fast digital curvelet transform (FDCT), which is less redundant, and has better performances than its predecessor. Curvelets have the capability of detecting the finest edges, those that can present more details in curvelet coefficients [31]. The application of curvelet can be found in many fields such as face detection [33], mammogram classification [34] and various other medical image classifications [35].

In a 2D space R^2 with a spatial variable x and frequency-domain variable w, the polar coordinates of the frequency-domain are r and θ. Curvelet transforms are defined by two windows, $W(r)$ and $V(t)$, called *radial window* and *angular window,* respectively [32]. These windows will always obey the following admissibility conditions:

$$\sum_{j=-\infty}^{\infty} W^2(2^j r) = 1 \quad r \in (3/4, 3/2) \tag{14}$$

$$\sum_{l=\infty}^{\infty} V^2(t - l) = 1 \quad t \in (-1/2, 1/2) \tag{15}$$

The frequency window U_j, in Fourier domain given by (16), represents a polar *wedge* supported by $W(t)$ and $V(t)$

$$U_j(r, \theta) = 2^{-3j/4}(2^{-j}r)V\left(\frac{2^{\lfloor j/2 \rfloor}}{2\pi}\right) \tag{16}$$

At scale 2^{-j}, orientation θ_l and position $x_k(j, l)$, the curvelet transform function of $\{x = (x_1, x_2)\}$ is given by (17)

$$\varphi_{j,l,k}(x) = \varphi_j\left(R_{\theta_l}\left(x - x_k^{(j,l)}\right)\right) \tag{17}$$

where R_θ is the rotation in radians and φ_j is the waveform and its Fourier transform is $\hat{\varphi}(w) = U_j(w)$. It is considered as *mother* curvelet in the sense that all curvelets are calculated by rotations and translations of φ_j [32].

Then, the curvelet coefficient, c given in (18), is obtained by the inner product between the element $f \in L^2(\boldsymbol{R}^2)$ and the curvelet transform $\varphi_{j,k,l}$

$$c(j, k, l) = \int_{\boldsymbol{R}^2} f(x)\overline{\varphi_{j,k,l}(x)}\,\mathrm{d}x\,. \tag{18}$$

There are two implementations of curvelet transforms, namely: unequispaced FFT and FDCT via wrapping (FDCT via wrapping). In the current paper, FDCT via wrapping has been implemented and a brief introduction is presented in Section 3.2.1

3.2.1 FDCTs via wrapping: FCDT via wrapping was introduced by Candes *et al.* [32] in their second generation of curvelet. This implementation is based on wrapping of Fourier samples with 2D image as input in Cartesian array form $f[m,n]$, where $0 \le m \le M$, $0 \le n \le N$, M and N are the dimensions of the array (image). Then, the discrete coefficients of FCDT are given below:

$$c^{\mathrm{D}}(j, l, k_1, k_2) = \sum_{0 \le m \le M,\, 0 \le n \le N} f[m, n]\varphi_{j,l,k_1,k_2}[m, n] \tag{19}$$

Equation (19) defines the digital curvelet coefficients. $c^{\mathrm{D}}(j, l, k_1, k_2)$ is indexed by a scale j, an orientation l and the spatial location parameters k_1 and k_2, where $\varphi_{j,l,k_1,k_2}^{\mathrm{D}}$ is the digital waveform.

Fig. 1 illustrates the advantages of curvelet transform in curve detection compared with WT [35]. It can be seen that for the same curve, curvelet transform needs less coefficients to fit widely the curve than WT. However, when the image has more dot singularities, the WT could give more performances.

3.3 LBP histogram features

LBPs operator is used for texture description. It is one of the best performing texture descriptors and it has been widely used in multiple applications [36, 37]. This operator was developed by Ojala *et al.* [38, 39]. Many variants of LBP were developed, for example, Heikkilä *et al.* [40] proposed centre-symmetric LBP, then, Zhang *et al.* [41] developed a new approach replacing the neighbour pixels by the mean of the neighbours' blocks, and Wolf *et al.* [42] proposed novel patches based LBP, where they explored the similarities between neighbouring patches of pixels. The majority of these developments is applied in face detection and recognition.

The LBP operator attributes for each pixel of the image a new value from 0 to 255 depending on its neighbourhood as explained below.

Let the image $I(x,y)$ and g_c denotes the grey level of an arbitrary pixel (x,y), *i.e.*$g_c = I(x, y)$. Moreover, let g_{p} denote the grey value of a sampling point in a circular neighbourhood space P and radius R around the point (x,y)

$$\begin{aligned} g_{\mathrm{p}} &= I(x_{\mathrm{p}}, y_{\mathrm{p}}) \quad p = 0, \ldots, P-1 \\ x_{\mathrm{p}} &= x + R\cos(2\pi p/P) \\ y_{\mathrm{p}} &= y - R\sin(2\pi p/P) \end{aligned}$$

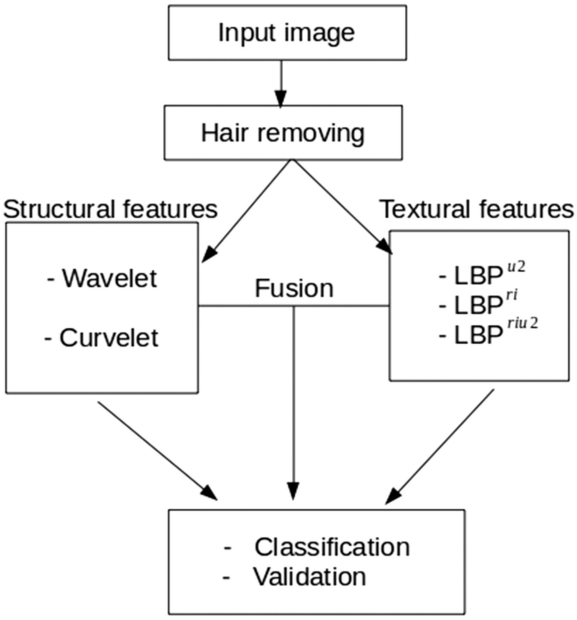

Fig. 2 *Main steps of the proposed method*

Table 2 Scoring system evaluation of ABCD rule [19]

Feature	Points (p_i)	Weight factor (w_i)	Sub-scoring range
asymmetry	0–2	1.3	0–2.6
border	0–8	0.1	0–0.8
colour	1–6	0.5	0.5–3
dermoscopic structures	1–5	0.5	0.5–2.5
total			1–8.9

Assuming that the local texture of the image $I(x,y)$ is characterised by the joint distribution $t(.)$ of grey values of $P+1$ ($P>0$) pixels

$$T = t(g_c, g_0, g_1, \ldots, g_{P-1}). \tag{20}$$

Without loss of information, the centre pixel value can be subtracted from the neighbourhood pixel values and (20) can be written as the following formula:

$$T = t(g_c, g_0 - g_c, g_1 - g_c, \ldots, g_{P-1} - g_c). \tag{21}$$

Assuming that the centre pixel is statistically independent to the differences, (21) is approximated by

$$T \simeq t(g_c)t(g_0 - g_c, g_1 - g_c, \ldots, g_{P-1} - g_c). \tag{22}$$

The important information is given by the differences distribution part *i.e.*$t(g_0 - g_c, g_1 - g_c, \ldots, g_{P-1} - g_c)$. However, the estimation of this distribution from image data is difficult. Ojala *et al.* [38] proposed to apply vector quantisation given by the following formula:

$$t(s(g_0 - g_c), s(g_1 - g_c), \ldots, s(g_{P-1} - g_c)). \tag{23}$$

where $s(z)$

$$s(z) = \begin{cases} 1 & z \geq 0 \\ 0 & z < 0. \end{cases} \tag{24}$$

Then, we can define the generic LBPs operator [43]

$$\mathrm{LBP}_{P,R}(x_c, y_c) = \sum_{p=0}^{P-1} s(g_p - g_c)2^p \tag{25}$$

According to Adjed *et al.* [44], the choices of $P=8$ and $R=1$ are the best cases for melanoma description.

Ojala *et al.* [39] introduced uniform pattern and invariant rotation LBP. Three variants were added, the first variant called uniform pattern indexed by LBP^{u2} keeps only the pattern containing a maximum of two transitions 0/1 and/or 1/0, this variant contains 59 combinations. The second is the invariant rotation pattern indexed by LBP^{ir}; it has the same configuration for all rotations, and it contains 36 combinations. The third variant is the invariant rotation uniform pattern indexed by LBP^{iru2}; it contains only the uniform patterns in the invariant rotation variant, indeed, it keeps only nine combinations.

4 Proposed method

The multitude of skin cancer lesions, benign and malignant, complicates the recognition of skin cancer. In addition to that, melanoma is developing randomly in different directions. Finding the best descriptor to discriminate melanoma is one of the challenging tasks in medical image processing. In the current paper, we present a set of discriminating features obtained from different descriptors to distinguish between benign and malignant cases as detailed in experimental work (Section 6). A detailed statistical analysis of the used database is also reported. The flowchart of the proposed feature extraction and fusion method is illustrated in Fig. 2. The methodology can be divided into two stages, i.e. computation of features (structural and texture) and fusion of features.

5 Database

PH^2 database was introduced in 2013 by Mendonca *et al.* [45] and more detailed in 2015 by the same authors [46]. PH^2 is a public and free database, built to perform and compare the evaluation of several systems. The database was built up through the joint collaboration between Universidade do Porto, Técnico Lisboa and the Dermatology service of Hospital Pedro Hispano in Matosinhos, Portugal. The acquisition of images was obtained under the same conditions. They are 8 bit RGB colour images with a resolution of 768×560 pixels.

The database contains a total of 200 dermoscopic images divided into 160 benign lesions and 40 melanomas. The benign lesions contain 80 common nevi and 80 atypical nevi. The quality, resolution and dermoscopic features of images are highlighted in the current database. Every image was segmented manually and diagnosed by several dermatologists. It contains also the clinical diagnosis and dermoscopic criteria such as asymmetry, colour and the presence of typical and atypical structures.

Table 2 summarises all the given characteristics in PH^2 database. It shows the percentage of the presence/absence of each characteristic. For each percentage, the number of images is noted between brackets. This table is to be read by columns, thus, for example, the common nevus is 96.25% fully symmetric, 2.5% is symmetric in one axis and only 1.25% is fully asymmetric and melanoma is 12.5% fully symmetric, 5% symmetric in one axis and 82.5% fully asymmetric. This table shows the dominant characteristics for each feature.

On the basis of the given features in Table 2, intuitively, the most difficult is to recognise the atypical nevus. Thus, for example, the asymmetry feature makes a real border between common nevus and melanoma only. The pigment network feature separates more common nevus with a total absence of pigment network to atypical and melanoma. However, the dots/globules features are not descriptive between the three cases. We can observe also that streaks and regression area features are more common in common nevus and atypical nevus than melanoma. Blue-whitish veil discriminates better between benign and malignant compared with other features. Finally, the colour increases gradually from common nevus to melanoma.

Another way of reading Table 2 is horizontally. Indeed, it shows the influence of each sub-feature. For example, the typical dot/globules feature is more frequently in common nevus than atypical

Table 3 Result of ABCD rule obtained from PH^2 database

Diagnositic parameter	Doliantilis *et al.*, %	PH^2 database, %
sensitivity	77.5	77.5
specificity	80.4	97.5
accuracy	73.2	87.5

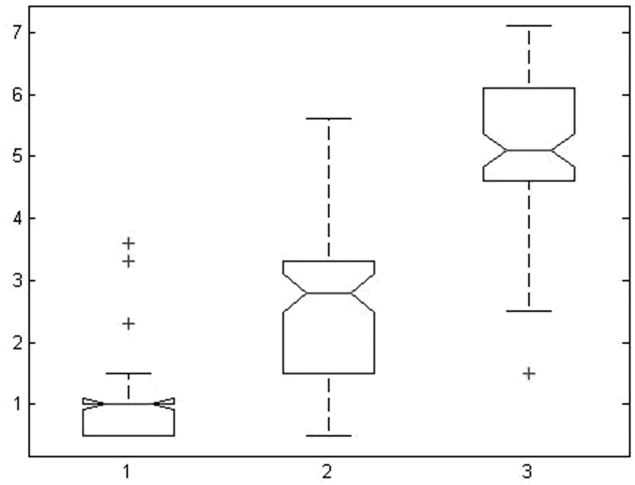

Fig. 3 *Variability of the three classes of the PH^2 database: (i) common nevus, (ii) atypical nevus, and (iii) melanoma*

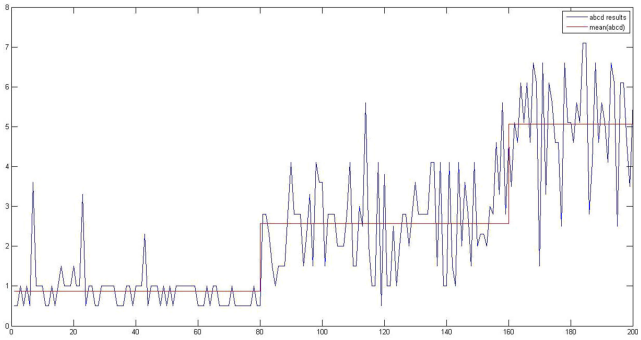

Fig. 4 *Results of ABCD rule system applied on PH^2 database*

nevus and almost inexistent in melanoma case. However, the atypical dot/globules feature shows an opposite behaviour with a high presence in melanoma, less in atypical nevus and rarely present in common nevus. A statistical analysis of the database is performed and compared with a based scoring system used in the hospitals in the next section.

5.1 Significance of the database

The informations given by the PH^2 database used in this paper contain all ABCD rules, except border irregularity scores, developed by Stolz *et al.* [10] and used for comparison by Capdehourat *et al.* [19] and Dolianitis *et al.* [47].

The PH^2 database quantifies each pigment following ABCD rule, excepting border irregularities. According to Capdehourat *et al.* [19], the evaluation of ABCD rule follows the scores summarised in Table 1, where dermoscopic structures contain pigment network, structures ares, dots, globules and branched streaks. The authors added to these features blue-whitish veil which is a major criteria of the 7-point checklist system [19].

Table 1 describes the Stolz's ABCD rule scoring system; it specifies a list of visual features associated with malignant lesions. Thus, the evaluation and the classification are done following the score value S attributed to each image, then it is classified as benign if ($S < 4.75$), clinical doubt lesion if $4.75 \leq S \leq 5.45$, or malignant if ($S > 5.45$). The function S is given by the following formula:

$$S = \sum_{i=0}^{4} p_i w_i \tag{26}$$

where p_i and w_i are the point value and the weight factor given in Table 1. This scoring system applied to the features described in Table 2 is same as used by Capdehourat *et al.* [19] where:

- Asymmetry is evaluated from 0 to 2, with 0 being fully symmetric, 1 for symmetric in one axis and 2 for fully asymmetric. It has the highest weight factor of 1.3.
- Border is evaluated with score from 0 to 8, drawing eight segments; one point is given for each abrupt pigment cutoff with a weight factor of 0.1.
- Colour is evaluated from 1 to 6, attributing one point for each colour with a weight factor of 0.5. Colours considered are white, red, black, light brown, dark brown and blue-grey.
- Dermoscopic structures encompass five structures which are: pigment network, structureless area, dots, globules and branched streaks. One point per structure with a weight factor of 0.5.

We note that there are some differences between extracted features in PH^2 database and ABCD rule. Therefore, the threshold of the scoring system is adapted removing the contribution of border irregularities. Then, the S score value of the function given in (26) is evaluated as follows: *benign*: if the score is $S < 4.50$; *clinical doubt*: lesion if the score lies between $4.50 \leq S \leq 5.20$; *malignant*: if the score is $S > 5.20$. There are other characteristic explored in the database such as blue-whitish veil, not used in ABCD rule, but used in another scoring system which is 7-points checklist [19]. However, the objective evaluation is difficult to be achieved due to the visual features characterised depending only on the decision of absence or presence of each characteristic.

The results reported by Dolianitis *et al.* are presented in Table 3. They are compared with the results obtained from PH^2 database applying ABCD rule. These results show a similar behaviour and equivalent results for the three performance metrics which are sensitivity, specificity and accuracy. As mentioned above, the threshold of ABCD rule, given in Table 1, applied on PH^2 database was adapted taking in consideration the missing values of border irregularities. Then, the value of the threshold is reduced to 4.5 and 5.20 instead of 4.75 and 5.45, respectively.

Analysis of variance is implemented on the vector obtained by ABCD rule by testing the H_0 (same population) against H_1 (different classes). The P-value obtained is <0.01, then, the hypothesis H_0 is significantly rejected with risk of 5%. Thus, the database presents significantly heterogeneous population (more than two classes).

The box plot in Fig. 3 illustrates graphically the variability of each group and deduces three different classes in the population. Fig. 4 describes the results of ABCD rule (blue) of the whole database and the mean of each class (red). Descriptively, using ABCD rule results, the graph shows more stability in common nevus lesion than the two other cases (atypical nevus and melanoma).

6 Experimental work

The proposed method detailed in Section 4 is applied on the 200 dermoscopic images from PH^2 database [46]. This database contains 160 non-melanoma (benign) and 40 melanoma (malignant) images. The classification is performed using SVM classifier with the linear kernel, 70% of the database is used for training and 30% for test. A random sampling cross-validation method is applied to validate the obtained results, where a thousand (1000) combinations of training and test sets are chosen randomly from the database. Thus, each image is used in average 700 times for training and 300 times for tests. An unbiased standard deviation (Std) for the thousand combinations is also computed for the three performance metrics (sensitivity, specificity and accuracy) detailed in the next section.

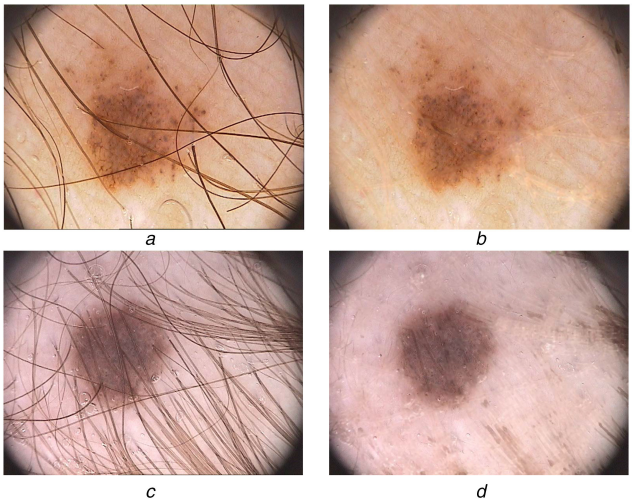

Fig. 5 *Hair removing with DullRazor software examples, applied on all images containing hairs*
(a) Original atypical nevus: IMD305 image, ***(b)*** Hair removing for IMD305 image, ***(c)*** Original common nevus: IMD003 image, ***(d)*** Hair removing for IMD003 image

6.1 Hair removing

To preprocess and enhance the image quality in the current paper, Dullrazor [Dullrazor software is available on http://www.dermweb.com/dull_razor/.] software is used for hair removing; it was applied on all the visible hairs as illustrated in Fig. 5. The statistical validity of dataset and robustness of the proposed approach is also explored in this paper.

6.2 Feature extraction

i. First, the structural features are extracted using wavelet and curvelet coefficients. Two-level decompositions of DWT and FDCT via warping (see Section 3.2.1) are applied on the melanoma ROIs. For each coefficient matrix, seven statistical features were computed, namely: *energy*, e*ntropy*, m*ean*, *Std*, m*aximum*, m*oment* and h*omogeneity*.
ii. Second, a set of textural features using different variants of LBP, i.e. rotationally invariant, uniform and non-uniform rotationally invariant distinct texture features are extracted.
iii. A feature fusion of structural and textural features is done.
iv. Finally, SVM classifier is used for classification and diagnosis. Then, 1000-random sampling cross-validation is explored to validate the obtained results.

- For wavelet, we used Daubechies 4 waveform, then eight coefficient matrices are computed, four from the first level and four from the second level (one approximation coefficient matrix and three detailed coefficient matrices) using (10)–(13). In total, we extracted 64 features from WTs.
- For two levels of curvelet decomposition nine curvelet coefficient matrices were obtained for each image, i.e. one matrix from the first level and eight matrices from the second level. These matrices are built using (19) detailed in the next section. Thus for each level, seven statistical features were computed. Thus, a total of 63 features from curvelet two-level decomposition were obtained.

For textural features, LBP operator is used to extract local textural variations. Thus, depending on the variant of LBP operator as detailed in Section 3.3, three LBP variants are explored in the current work. Therefore, we have:

- 59 textural features from LBP^{u2} (uniform pattern).
- 36 from LBP^{ri} (invariant rotation).
- 9 from LBP^{riu2} (invariant rotation uniform pattern).

Indeed, we used only radius $R = 1$ and eight neighbourhood pixels ($P = 8$), this choice is concluded from our previous work [44], where the results obtained showed a better performance for $R = 1$ and $P = 8$. Here, it is worth mentioning that all the features were normalised to the range [0–1] and their influence before and after fusion can be recorded in validation performances.

7 Experimental results

The evaluation of the proposed method is measured using three performance metrics which are sensitivity (*sen*), specificity (*spe*) and accuracy (*acc*) [7], as given in (27)–(29)

$$\mathrm{sen} = \frac{\mathrm{TP}}{\mathrm{TP} + \mathrm{FN}} \tag{27}$$

$$\mathrm{spe} = \frac{\mathrm{TN}}{\mathrm{TN} + \mathrm{FP}} \tag{28}$$

$$\mathrm{acc} = \frac{\mathrm{TP} + \mathrm{TN}}{\mathrm{TP} + \mathrm{FN} + \mathrm{TN} + \mathrm{FP}} \tag{29}$$

where true positives (TPs) define the melanoma classified as melanoma, true negatives (TNs) defines the non-melanoma classified as non-melanoma, false positives (FPs) and false negatives (FNs) are the melanoma and non-melanoma which are not classified on the right set, respectively.

Equation (29) depends on the number of benign and malignant lesions. To remove this dependence, we estimate the accuracy in the following way:

$$\hat{\mathrm{acc}} = \frac{\alpha\mathrm{TP} + \mathrm{TN}}{\alpha\mathrm{TP} + \alpha\mathrm{FN} + \mathrm{TN} + \mathrm{FP}} \tag{30}$$

The parameter α is added to compensate the difference of images number in the accuracy performance. This parameter is obtained by the following formula:

$$\alpha = \frac{\#\mathrm{Benign}}{\#\mathrm{Malignant}} \tag{31}$$

where *#Benign* and *#Malignant* design the number of benign and malignant images, respectively. Therefore, $\alpha = 2$ for the first and second classifications (melanoma versus atypical and melanoma versus common nevus) and $\alpha = 4$ for the last classification (malignant and benign lesions). The performance results are computed also by accuracy given by (30). Equation (30) can be also used with different values of the parameter α to give more weight for FNs or FPs to tolerate or reject some special situations such as let cancerous patients without treatment which are FNs. In our case, the α chosen is used just to regulate the difference between benign and malignant lesions. This formulation is equivalent to $(sen + spe)/2$ used in Barata *et al.* [28]. In the next section, the results show a significant difference between the two metrics.

Fig. 6*a* presents the evolution of the modified accuracy ($\hat{\mathrm{acc}}$) depending on different values of α, from 0.1 to 5, fixing others variables (sensitivity, specificity, malignant number and benign number), whereas Fig. 6*b* illustrates the dependence of the accuracy metric (29) on malignant and benign numbers, presented by the dark curve. By varying the β value from 0.1 to 5 in $M = \beta B$, where M is the malignant number, B is the benign number, we can see easily that the accuracy (acc) is strongly dependent on those quantities. The blue colour line presents the modified accuracy ($\hat{\mathrm{acc}}$), with $\alpha = 1/\beta$, to compensate the difference between malignant and benign numbers.

Knowing that the database is presented in three different classes: common nevus, atypical nevus and melanoma. Then, to have a representative training set, 70% of each class (common and atypical) is taken for training and the other 30% for test. This choice guarantees the representativeness of atypical and common nevus in training and test sets.

To detect melanoma lesions, the results are classified into three cases. First, we explored the classification between melanoma and atypical nevus. Second, we explored classification performance between melanoma and common nevus and finally we performed the classification between melanoma and the whole benign lesions. Three performance metrics, i.e. sensitivity, specificity and accuracy/modified accuracy given by the (**27**)–(**30**) are computed. For each performance, we compute also 1000-random combinations for the choice of the training and test sets. In the result Tables 4–6, Validation Performance (VP) defines the validation performance and Std represents the standard deviation of the thousand combinations used for validation. The results are divided into three categories which are textural features using LBP operator, structural features using wavelet and curvelet coefficients and finally the mixture of textural and structural features.

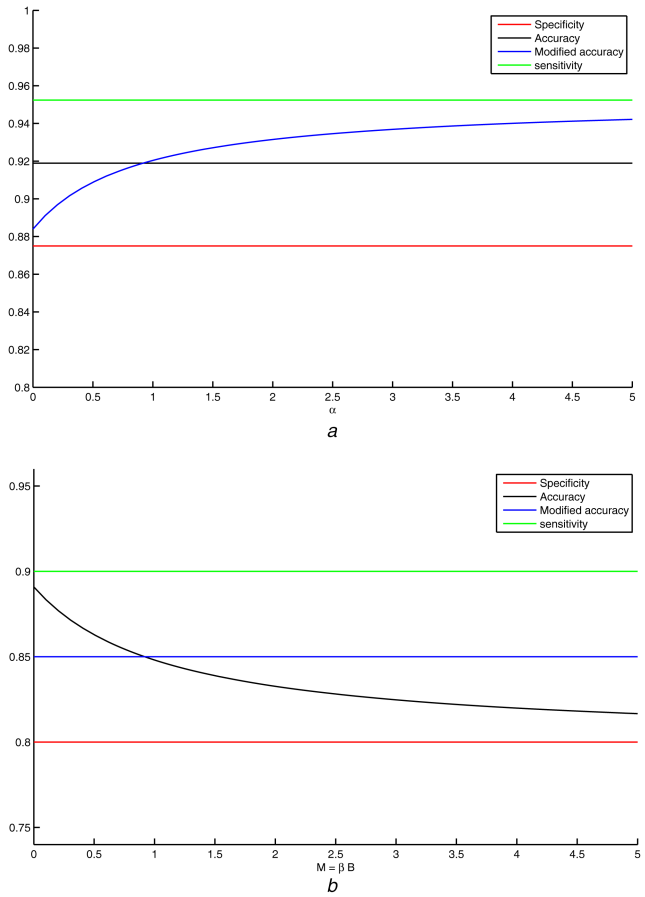

Fig. 6 *Illustration of the modified accuracy effect's on the obtained result using the formula given by (30)*
(a) Modified accuracy ($a\hat{c}c$) in function of α, presented by blue colour, ***(b)*** Accuracy (acc) depending on the number of malignant and benign lesions, presented by the dark colour

7.1 Melanoma versus atypical nevus

In this section, the classification is focused on the detection and the recognition of melanoma mixed only with atypical nevus, those presented by the second and the third columns in Table 2. The results obtained are given in Table 4. Therefore, for textural features, the best performances are obtained by LBP^{u2} followed by the LBP^{ir}, and the worst result is obtained by the LBP^{riu2}. For structural features, wavelet shows better results than curvelet for all metrics performances used. The fusion of textural and structural features gives better results in wavelet coefficients with LBP operator and it shows a smallest Std for the variability of validation results expressed by the variable Std. Wavelet with LBP^{u2} improves the three metrics used and gives the best results compared with all the methods studied. The fusion of curvelet coefficients with LBP operator improves the specificity metric compared with curvelet and LBP separately.

7.2 Melanoma versus common nevus

As mentioned above, the second classification is done only between melanoma and common nevus lesions. Table 5 shows the performance validation of sensitivity, specificity and accuracies metrics. For textural features, LBP^{ri} and LBP^{u2} show a higher performance than LBP^{riu2}, and we can see that LBP^{ri} is more sensitive and less specific than LBP^{u2}. The textural features performances show that wavelet coefficients discriminate melanoma better than curvelet coefficients and the fusion LBP operator contributes in the reduction of the variability between different combinations in validation step.

It can be seen that the best results validation are performed using wavelet and the fusion of wavelet with different variants of LBP. The fusion of wavelet and LBP^{u2} is the most stable operator showing the smallest Std value for the three metrics.

7.3 Melanoma versus atypical and common nevus

In this section, the classification is performed between malignant and benign (atypical and common nevus) lesions. The results are presented in Table 5. Thus, for textural features, we can see that LBP^{ri} is more sensitive and more accurate than LBP^{riu2} and LBP^{u2}. The opposite results are obtained for specificity, where LBP^{u2} gives the highest value and the smallest variation compared with the other variants of LBP. The accuracy obtained from the validation results is higher than 81% for both LBP^{ri} and LBP^{u2} variants.

Table 4 Results obtained for melanoma versus atypical nevus giving performance validation VP and the Std for 1000-random-cross-validation under SVM classifier

Performances metrics		Sensitivity (*sen*)		Specificity (*spe*)		Accuracy (*acc*)		Accuracy ($a\check{c}c$)	
Features	Methods	VP, %	Std	VP, %	Std	VP, %	Std	VP, %	Std
textural features	LBP^{ri}	77.44	11.88	81.97	8.04	80.46	5.82	79.70	6.30
	LBP^{riu2}	74.17	12.09	73.19	9.29	73.51	6.77	73.68	6.83
	LBP^{u2}	76.55	12.32	85.15	7.35	82.28	5.56	80.85	6.31
structural features	wavelet	79.47	12.93	88.99	7.10	85.79	6.07	84.23	6.84
	curvelet	73.10	13.56	82.01	7.56	79.04	6.14	77.56	6.85
fusion of structural and textural features	wavelet + LBP^{ri}	78.13	12.08	88.63	6.90	85.11	5.49	83.38	6.42
	wavelet + LBP^{riu2}	77.51	12.37	88.22	5.80	84.62	5.80	82.86	6.81
	wavelet + LBP^{u2}	81.84	11.29	88.57	6.80	86.31	5.48	85.20	6.24
	curvelet + LBP^{ri}	79.08	12.50	85.69	7.34	83.49	5.72	82.38	6.08
	Curvelet + LBP^{riu2}	76.15	13.31	82.84	7.66	80.61	6.25	79.49	6.83
	curvelet + LBP^{u2}	78.75	11.89	86.83	6.89	84.14	5.51	82.79	6.30
wavelet + curvelet		78.97	12.84	85.51	7.14	83.98	6.01	82.24	6.87

Table 5 Results obtained for melanoma versus common nevus giving performance validation VP and the Std for the 100-random-cross-validation under SVM classifier

Performances metrics		Sensitivity (*sen*)		Specificity (*spe*)		Accuracy (*acc*)		Accuracy ($\widetilde{acc}$)	
Features	Methods	VP, %	Std	VP, %	Std	VP, %	Std	VP, %	Std
textural features	LBP^{ri}	82.28	11.11	84.29	7.71	83.62	5.72	83.29	5.88
	LBP^{riu2}	78.92	12.07	77.68	8.35	78.09	6.16	78.30	6.40
	LBP^{u2}	80.82	12.56	87.80	6.78	85.47	5.74	84.31	6.70
structural features	wavelet	88.47	10.36	91.99	5.67	90.81	5.23	90.23	5.65
	curvelet	80.80	12.25	84.53	7.63	83.29	6.20	82.66	6.58
fusion of structural and textural features	wavelet + LBP^{ri}	88.82	9.44	90.95	5.93	90.24	4.97	89.88	5.15
	wavelet + LBP^{riu2}	88.91	10.06	91.45	5.85	90.60	4.99	90.17	5.54
	wavelet + LBP^{u2}	89.25	9.26	90.80	5.59	90.28	4.76	90.02	4.92
	curvelet + LBP^{ri}	81.25	11.36	85.68	7.30	84.20	5.76	83.47	5.25
	curvelet + LBP^{riu2}	81.64	11.93	85.34	7.40	84.11	6.23	83.49	6.53
	curvelet + LBP^{u2}	82.86	11.12	87.17	6.86	85.73	5.48	85.02	6.03
wavelet + curvelet		87.73	10.57	90.40	6.99	89.51	5.68	89.06	6.19

Table 6 Results obtained for melanoma versus atypical and common nevus giving performance validation VP and the Std for the 100-random-cross-validation under SVM classifier

Performances metrics		Sensitivity (*sen*)		Specificity (*spe*)		Accuracy (*acc*)		Accuracy ($\widetilde{acc}$)	
Features	Methods	VP, %	Std	VP, %	Std	VP, %	Std	VP, %	Std
textural features	LBP^{ri}	78.07	12.35	86.14	4.80	84.53	3.89	82.10	5.90
	LBP^{riu2}	77.74	11.29	75.95	5.92	76.31	4.67	76.84	6.02
	LBP^{u2}	74.13	13.01	89.40	4.52	86.34	3.82	81.76	6.28
structural features	wavelet	77.56	13.17	93.50	3.48	90.31	3.44	85.54	6.54
	curvelet	70.42	14.50	89.29	4.91	85.52	4.41	79.85	7.18
fusion of structural and textural features	wavelet + LBP^{ri}	75.42	13.68	93.46	3.65	89.85	3.52	84.41	6.79
	wavelet + LBP^{riu2}	76.73	13.49	93.47	3.59	90.12	3.44	85.08	6.67
	wavelet + LBP^{u2}	78.93	11.95	93.25	3.61	90.34	3.27	86.07	6.32
	curvelet + LBP^{ri}	72.35	13.34	90.56	4.41	86.92	3.81	81.46	6.55
	curvelet + LBP^{riu2}	70.30	14.76	89.19	4.72	85.38	4.24	79.74	7.13
	curvelet + LBP^{u2}	72.67	12.88	91.09	3.99	87.40	3.61	81.88	6.46
wavelet + curvelet		76.16	14.11	93.13	3.68	89.74	3.95	84.64	6.99

For structural features, in our case, the wavelet coefficient shows a better performance compared with curvelet coefficients with an accuracy performance of 85.54 and 79.85%.

The fusion of the wavelet and LBP^{u2} increases considerably the specificity and the accuracy performances as shown in Table 6. However, the fusion does not show any significant effect on sensitivity performance.

The best results for all the performances metrics validation is obtained by the fusion of wavelet coefficients and LBP^{u2} with 78.93% of sensitivity validation, 93.25 of specificity validation and 86.07% of accuracy validation.

7.4 Results analysis

From Tables 4–6, we can deduce by using the two sets of features (textural and structural) that the detection of melanoma mixed with common nevus is easier as compared with melanoma mixed with atypical nevus, which is expected as the class overlap between melanoma and common nevus is less than that between melanoma and atypical nevus. Thus, the stability of common nevus is illustrated in Fig. 4 and presented by the result obtained in Table 5 with a highest accuracy of 90%. We can conclude that the detection and the recognition performances of melanoma depends on the kind of the benign lesions used for computation.

The fusion of wavelet and LBP^{u2} outperforms all the tested methods in the current work, as it can be seen from the results in Tables 4–6. In general, curvelets have better performances than wavelets. However, in our case, the results obtained show better performances from wavelet coefficients compared with curvelet coefficients in the three tables. These results can be explained by the multitude of singularity points coming from the random development of skin cancer lesions. It could also be expressed by the redundancy of curvelet coefficients which represent the double of the redundancy of wavelet coefficients [48].

As detailed in Sections 3.1 and 3.2, the wavelet is efficient for singularity points and curvelet is more efficient for the detection or characterisation of curves. Therefore, we also evaluate a fusion between the two sets of coefficients as Li *et al.* [49] used for image compression. Thus, the results obtained are not showing any significant improvement in the detection.

Table 7 presents a comparison of the proposed method with recent works on classification and recognition of melanoma using the same database PH^2. Our proposed method shows the highest performance in terms of specificity and accuracy compared with Barata *et al.* [28], showing a validated result of 93 and 86%, respectively. Although accuracy is higher for Abuzaghleh *et al.* proposition [25], they did not perform any validation comparing neither the current work validated by *n*-random sampling cross-validation, nor *k*-fold cross-validation used by Barata *et al.* In addition to this, the authors used 75% of the database for training in place of 70% frequently used in the literature. The authors used the fusion of FFT with DCT, and their results are still less efficient than the proposed method (see Table 7), because the authors did not present sensitivity and specificity performances, and no information on training and test sets is presented. Therefore, it is difficult to reproduce the same result for comparison. Furthermore, knowing that the benign lesions are heterogeneous [3], then, if we choose some special configurations of training and test sets we

Table 7 Comparison of the results of the proposed approach with the results of recent methods in the literature using the same database

Method	Method used	Sensitivity, %	Specificity, %	Accuracy, %
Barata *et al.* [28]	four algorithms to extract colour constancy (Gray World, max-RGB, Shady of Gray and General Gray World). SVM classifier with the χ^2 kernel is used for classification on PH^2 database	92.5	76.3	84.3
Abuzaghleh *et al.* [25]	the authors used colour and shape geometry features using FFT and DCT. SVM classifier is used on PH^2 database for 75% for training and 25% for test	—	—	90.6
proposed method	a fusion textural and structural features. Results of random sampling cross-validation under SVM classifier with the linear kernel used for classification on PH^2 database with 70% for training and 30% for test	78.93	93.25	86.07

could present higher results than those presented in Tables 4–6. Thus, the validation result step is crucial for the adaptability of the proposed method.

The known ABCD rule, often used in hospitals manually, has achieved an accuracy of 87.5% as in Table 3. In this work, the proposed automation of the ABCD rule achieved an accuracy of 86.07% as in Table 7, which is fairly comparable with the result obtained manually. This achievement shows a great potential of developing CAD system for melanoma detection.

8 Conclusion

In this paper, fusion of structural and textural features is explored for melanoma recognition. The structural features are obtained from the first and second levels of wavelet and curvelet coefficients, and the textural features are obtained from the different variants of LBP operator. The best results are performed by the fusion of wavelet coefficients and LBP^{u2}. The obtained results are also validated using random sampling cross-validation under SVM classifier with linear kernel on PH^2 dermoscopy database. The proposed methods show great potential results in terms of sensitivity, specificity and accuracy metrics.

As suggested in the literature [50], it is important to provide the necessary details of the methods presented, for example, the configuration parameters and algorithms. In addition, a random sampling cross-validation is performed using 1000-random combinations of training and test sets from the database. The validation step is necessary and important for robustness of the proposed method.

For a systematic comparison between research methods, the use of a free public database is required. Therefore, we used the first, unique and complete public database published by Mendonça *et al.* [46]. Another huge public database is available (but still under development) proposed in ISIC archive [51], the clinical informations and the border segmentation lesions are not yet completely available.

9 References

[1] World Health Organization: 'How common is skin cancer?', 2015. Available at, http://www.who.int/uv/faq/skincancer/en/index1.html, accessed on 18 August 2016

[2] ©Les cancer en France en 2013: 'Collection état des lieux et des connaissances, ouvrage collectif édité par l'inca', January 2014. Available at http://www.e-cancer.fr/Expertises-et-publications/Catalogue-des-publications/Les-cancers-en-France-Edition-2013

[3] Fundation, S.C.: 'Skin cancer information', 2016. Available at, http://www.skincancer.org/skin-cancer-information, accessed on 20 August 2016

[4] Arroyo, J.L.G., Zapirain, B.G.: 'Detection of pigment network in dermoscopy images using supervised machine learning and structural analysis', *Comput. Biol. Med.*, 2014, **44**, pp. 144–157

[5] Cancer Research UK: 'Treating skin cancer', 2016. Available at http://www.cancerresearchuk.org/about-cancer/type/skin-cancer/treatment/, accessed on 14 October 2016

[6] Korotkov, K., Garcia, R.: 'Computerized analysis of pigmented skin lesions: a review', *Artif. Intell. Med.*, 2012, **56**, (2), pp. 69–90

[7] Celebi, M.E., Wen, Q., Iyatomi, H., *et al.*: '*A state-of-the-art survey on lesion border detection in dermoscopy images*' (CRC Press, Boca Raton, 2015)

[8] Lee, T., Ng, V., Gallagher, R., *et al.*: 'Dullrazor: a software approach to hair removal from images', *Comput. Biol. Med.*, 1997, **27**, (6), pp. 533–543

[9] Barata, C., Ruela, M., Francisco, M., *et al.*: 'Two systems for the detection of melanomas in dermoscopy images using texture and color features', *IEEE Syst. J.*, 2014, **8**, (3), pp. 965–979

[10] Stolz, W., Riemann, A., Cognetta, A., *et al.*: 'ABCD rule of dermatoscopy-a new practical method for early recognition of malignant melanoma', *Eur. J. Dermatol.*, 1994, **4**, (7), pp. 521–527

[11] Argenziano, G., Fabbrocini, G., Carli, P., *et al.*: 'Epiluminescence microscopy for the diagnosis of doubtful melanocytic skin lesions: comparison of the ABCD rule of dermatoscopy and a new 7-point checklist based on pattern analysis', *Arch. Dermatol.*, 1998, **134**, (12), pp. 1563–1570

[12] Abbas, Q., Garcia, I.F., Emre Celebi, M., *et al.*: 'A feature-preserving hair removal algorithm for dermoscopy images', *Skin Res. Technol.*, 2013, **19**, (1), pp. e27–e36

[13] Barata, C., Marques, J.S., Rozeira, J.: 'A system for the detection of pigment network in dermoscopy images using directional filters', *IEEE Trans. Biomed. Eng.*, 2012, **59**, (10), pp. 2744–2754

[14] Koehoorn, J., Sobiecki, A.C., Boda, D., *et al.*: 'Automated digital hair removal by threshold decomposition and morphological analysis'. Int. Symp. Mathematical Morphology and its Applications to Signal and Image Processing, 2015, pp. 15–26

[15] Mirzaalian, H., Lee, T.K., Hamarneh, G.: 'Hair enhancement in dermoscopic images using dual-channel quaternion tubularness filters and MRF-based multilabel optimization', *IEEE Trans. Image Process.*, 2014, **23**, (12), pp. 5486–5496

[16] Frangi, A.F., Niessen, W.J., Vincken, K.L., *et al.*: 'Multiscale vessel enhancement filtering'. Int. Conf. Medical Image Computing and Computer-Assisted Intervention, 1998, pp. 130–137

[17] Celebi, M.E., Iyatomi, H., Schaefer, G., *et al.*: 'Lesion border detection in dermoscopy images', *Comput. Med. Imaging Graph.*, 2009, **33**, (2), pp. 148–153

[18] Celebi, M.E., Kingravi, H.A., Uddin, B., *et al.*: 'A methodological approach to the classification of dermoscopy images', *Comput. Med. Imaging Graph.*, 2007, **31**, (6), pp. 362–373

[19] Capdehourat, G., Corez, A., Bazzano, A., *et al.*: 'Toward a combined tool to assist dermatologists in melanoma detection from dermoscopic images of pigmented skin lesions', *Pattern Recognit. Lett.*, 2011, **32**, (16), pp. 2187–2196

[20] Safi, A., Baust, M., Pauly, O., *et al.*: 'Computer-aided diagnosis of pigmented skin dermoscopic images'. MICCAI Int. Workshop on Medical Content-Based Retrieval for Clinical Decision Support, 2011, pp. 105–115

[21] Li, F., Shen, C., Li, C.: 'Multiphase soft segmentation with total variation and h1 regularization', *J. Math. Imaging Vis.*, 2010, **37**, (2), pp. 98–111

[22] Chan, T.F., Vese, L.A.: 'Active contours without edges', *IEEE Trans. Image Process.*, 2001, **10**, (2), pp. 266–277

[23] Adjed, F., Faye, I., Ababsa, F.: 'Segmentation of skin cancer images using an extension of chan and vese model'. 2015 Seventh Int. Conf. Information Technology and Electrical Engineering (ICITEE), 2015, pp. 442–447

[24] Clawson, K.M., Morrow, P., Scotney, B., *et al.*: 'Analysis of pigmented skin lesion border irregularity using the harmonic wavelet transform'. 13th Int. Machine Vision and Image Processing Conf. 2009 IMVIP'09, 2009, pp. 18–23

[25] Abuzaghleh, O., Barkana, B.D., Faezipour, M.: 'Automated skin lesion analysis based on color and shape geometry feature set for melanoma early detection and prevention'. 2014 IEEE Long Island Systems, Applications and Technology Conf. (LISAT), 2014, pp. 1–6

[26] Maglogiannis, I., Doukas, C.N.: 'Overview of advanced computer vision systems for skin lesions characterization', *IEEE Trans. Inf. Technol. Biomed.*, 2009, **13**, (5), pp. 721–733

[27] Codella, N., Cai, J., Abedini, M., *et al.*: 'Deep learning, sparse coding, and SVM for melanoma recognition in dermoscopy images'. Int. Workshop on Machine Learning in Medical Imaging, 2015, pp. 118–126

[28] Barata, C., Celebi, M.E., Marques, J.S.: 'Improving dermoscopy image classification using color constancy', *IEEE J. Biomed. Health Inf.*, 2015, **19**, (3), pp. 1146–1152

[29] Grossmann, A., Morlet, J.: 'Decomposition of hardy functions into square integrable wavelets of constant shape', *SIAM J. Math. Anal.*, 1984, **15**, (4), pp. 723–736

[30] Mallat, S.G.: 'A theory for multiresolution signal decomposition: the wavelet representation', *IEEE Trans. Pattern Anal. Mach. Intell.*, 1989, **11**, (7), pp. 674–693

[31] Candes, E.J., Donoho, D.L.: '*Curvelets: a surprisingly effective nonadaptive representation for objects with edges*' (Stanford University, Department of Statistics, 2000)

[32] Candes, E., Demanet, L., Donoho, D., *et al.*: 'Fast discrete curvelet transforms', *Multiscale Model. Simul.*, 2006, **5**, (3), pp. 861–899

[33] Mandal, T., Majumdar, A., Wu, Q.J.: 'Face recognition by curvelet based feature extraction'. Int. Conf. Image Analysis and Recognition, 2007, pp. 806–817

[34] Gardezi, S., Faye, I.: 'Fusion of completed local binary pattern features with curvelet features for mammogram classification', *Appl. Math. Inf. Sci.*, 2015, **9**, (6), pp. 3037–3048
[35] Alzubi, S., Islam, N., Abbod, M.: 'Multiresolution analysis using wavelet, ridgelet, and curvelet transforms for medical image segmentation', *J. Biomed. Imaging*, 2011, **2011**, p. 4
[36] Ahonen, T., Hadid, A., Pietikäinen, M.: 'Face description with local binary patterns: application to face recognition', *IEEE Trans. Pattern Anal. Mach. Intell.*, 2006, **28**, (12), pp. 2037–2041
[37] Porebski, A., Vandenbroucke, N., Macaire, L.: 'Haralick feature extraction from LBP images for color texture classification'. 2008 First Workshops on Image Processing Theory, Tools and Applications, 2008, pp. 1–8
[38] Ojala, T., Valkealahti, K., Oja, E., *et al.*: 'Texture discrimination with multidimensional distributions of signed gray-level differences', *Pattern Recognit.*, 2001, **34**, (3), pp. 727–739
[39] Ojala, T., Pietikainen, M., Maenpaa, T.: 'Multiresolution gray-scale and rotation invariant texture classification with local binary patterns', *IEEE Trans. Pattern Anal. Mach. Intell.*, 2002, **24**, (7), pp. 971–987
[40] Heikkilä, M., Pietikäinen, M., Schmid, C.: 'Description of interest regions with center-symmetric local binary patterns'. ICVGIP, 2006, vol. **6**, pp. 58–69
[41] Zhang, L., Chu, R., Xiang, S., *et al.*: 'Face detection based on multi-block LBP representation'. Advances in biometrics, 2007, pp. 11–18
[42] Wolf, L., Hassner, T., Taigman, Y.: 'Descriptor based methods in the wild'. Workshop on Faces in 'Real life' images: Detection, Alignment, and Recognition, 2008
[43] Pietikäinen, M., Hadid, A., Zhao, G., *et al.*: '*Computer vision using local binary patterns*', vol. **40** (Springer Science & Business Media, 2011)
[44] Adjed, F., Faye, I., Ababsa, F., *et al.*: 'Classification of skin cancer images using local binary pattern and SVM classifier'. AIP Conf. Proc., 2016, vol. **1787**, p. 080006
[45] Mendonca, T., Ferreira, P.M., Marques, J.S., *et al.*: 'PH^2 – a dermoscopic image database for research and benchmarking'. 2013 35th Annual Int. Conf. the IEEE Engineering in Medicine and Biology Society (EMBC), 2013, pp. 5437–5440
[46] Mendonça, T.F., Ferreira, M.P., Marcal, A.R.S., *et al.*: 'PH2: a public database for the analysis of dermoscopic images', in Celebi, M.E., Mendonca, T., Marques, J.S. (EDs.): '*Dermoscopy image analysis*' (CRC Press, 2015, vol. **10**), pp. 419–439
[47] Dolianitis, C., Kelly, J., Wolfe, R., *et al.*: 'Comparative performance of 4 dermoscopic algorithms by nonexperts for the diagnosis of melanocytic lesions', *Arch. Dermatol.*, 2005, **141**, (8), pp. 1008–1014
[48] Fadili, J.M., Starck, J.L.: '*Curvelets and ridgelets*' (Springer New York, 2009)
[49] Li, S., Yang, B.: 'Multifocus image fusion by combining curvelet and wavelet transform', *Pattern Recognit. Lett.*, 2008, **29**, (9), pp. 1295–1301
[50] Celebi, M.E., Mendonca, T., Marques, J.S.: '*Dermoscopy image analysis*', vol. **10** (CRC Press, 2015)
[51] Database, I.A.: 'ISIC archive: international skin imaging collaboration', accessed on 27 February 2017